Available online at www.sciencedirect.com
ScienceDirect
Journal of Power Sources 177 (2008) 273–280
JOURNAL OF POWER SOURCES
www.elsevier.com/locate/jpowsour

Electron microscopy techniques for the analysis of the polymer electrolyte distribution in proton exchange membrane fuel cells

Frieder Scheiba [a,*], Nathalie Benker [b], Ulrike Kunz [a], Christina Roth [a], Hartmut Fuess [a]

[a] *Institute for Materials Science, Darmstadt University of Technology, Petersenstr. 23, D-64287 Darmstadt, Germany*
[b] *Institute for Applied Geosciences, Darmstadt University of Technology, Schnittspahnstr. 9, D-64287 Darmstadt, Germany*

Received 8 October 2007; received in revised form 21 November 2007; accepted 24 November 2007
Available online 3 December 2007

Abstract

The polymer electrolyte distribution in PEMFC electrodes plays an important role for the catalyst utilization and various transport processes in the electrode. Moreover, its influence on the transport processes is not only limited to proton transport but it may also affect gas transport, electron conductivity and water management of the cell. However, experimental techniques to study the polymer electrolyte distribution are scarce. In this paper we present various approaches based on scanning electron microscopy (SEM) and transmission electron microscopy (TEM) to characterize the polymer electrolyte distribution. The methods presented include staining of the polymer electrolyte with heavy metal ions, energy dispersive X-ray (EDX) mapping and energy filtered imaging (EFI). Their use for the analysis of the polymer electrolyte distribution and electrode structure will be presented and current limitations of these techniques will be discussed.

Keywords: PEMFC; Polymer electrolyte; Ionomer; Distribution; EF-TEM; EDX mapping; Microtomy

1. Introduction

Transport processes play a significant role for the proper operation of polymer electrolyte membrane fuel cells (PEMFCs). In PEMFCs the reactant gases (i.e. hydrogen on the anode and oxygen on the cathode) must have access to the catalytically active sites, protons and electrons must be conducted through the electrode and the reaction product water must be removed from the pore system to avoid blocking of the gas diffusion paths.

In the current standard electrode design each transport process is realized by a different component. Gas transport is accomplished by a network of pores in the electrode structure. Electrons are conducted by the catalyst particles themselves or a conductive support, whereas proton diffusion is realized by the addition of a polymer electrolyte. Furthermore, PTFE is often added to the electrode, especially the cathode side, to increase its hydrophobicity, which enhances the removal of reaction water from the pore system [1–3].

Since the various components influence each other and therefore the electrode properties in a nonconstructive manner, optimization of the electrode structure is far from being trivial.

One of the key components in electrode design is the polymer electrolyte, because it influences proton conductivity as well as the catalysts electrochemically active surface, mass transport, electronic resistivity and electrode porosity.

Several publications have focused on the effect of the polymer electrolyte concentration in the electrode [4–8]. Generally intermediate contents of 30–40 wt.% are reported as optimal concentrations for perfluorosulfonated ionomers (PFSI) such as Nafion® and Flemion® with carbon black supported catalysts [4–7]. At low and high electrolyte contents a much poorer electrode performance is observed. For low electrolyte contents the moderate electrode performance is explained by limited proton conductivity and incomplete wetting of catalyst by the ionomer which decreases the electrochemically active surface [4,5]. Whereas at high electrolyte contents exceeding 40 wt.% the pore size and average pore diameter decrease dramatically, and the electrode performance becomes diffusion controlled [5,7].

Beside the absolute amount of polymer electrolyte in the electrode, its distribution has a significant effect on the performance

* Corresponding author. Tel.: +49 6151 165498; fax: +49 6151 166023.
E-mail address: scheiba@st.tu-darmstadt.de (F. Scheiba).

0378-7753/$ – see front matter © 2007 Elsevier B.V. All rights reserved.
doi:10.1016/j.jpowsour.2007.11.085

of the cell. The distribution of the electrolyte is mainly influenced by the preparation technique of the electrode, i.e. the catalyst ink preparation and coating procedure. For instance several authors report an increased electrode performance, when PFSI is dispersed in a solvent where it forms a colloidal solution [9–11]. Based on mercury porosimetry measurements Shin et al. conclude that the PFSI in the colloidal state does only penetrate into the pore range between 0.07 and 1 μm, while the pores smaller than 0.07 μm remained almost unaffected [10]. In contrast, when the PFSI was used in its solubilized state mainly the pore volume of pores smaller than 0.07 μm was reduced, unless very high PFSI concentrations were used in the electrode. The pore range between 0.07 and 1 μm is generally attributed to pores in between the catalyst agglomerates, while the pore range below 0.07 μm is attributed to the pores in the agglomerates themselves [11]. Influences of the coating technique on the PFSI distribution were reported recently by Xie et al. [12]. They demonstrated that for the decal technique [13] the choice of the decal substrate has a significant effect on the polymer electrolyte distribution. Electrodes prepared on PTFE substrates had an approximately 0.7 μm thick Nafion® layer on the substrate side, while electrodes prepared on less hydrophobic substrates (Kapton) did not show Nafion® layers. The layer on the PTFE substrate was explained by interaction of the hydrophobic polytetrafluoroethylene backbones of the ionomer with the PTFE substrate. The Nafion® layer was found to impose mass-transport limitations especially in the high current regime.

However, detailed analysis of the polymer electrolyte distribution is difficult. Mercury porosimetry which has been widely used to study the influence of various preparation parameters on the pore size distribution, may in some cases be used to derive information on the polymer electrolyte distribution. But since mercury porosimetry probes the pore size distribution rather than the polymer electrolyte distribution itself, information on the polymer electrolyte distribution requires the choice of an appropriate reference and is based on the assumption that differences in the pore size distribution are directly correlated with the polymer electrolyte distribution. Scanning electron microscopy (SEM), which is also commonly used for structural characterization of the electrode, may in principle be used to obtain direct information on the polymer electrolyte distribution if it is combined with energy dispersive X-ray analysis (EDX) [14]. However, SEM on bulk electrodes has a number of limitations. Due to the high porosity and low density of the carbon support material the electron beam penetrates deeply into the sample. This limits the obtainable resolution for Z-contrast back scattered electrons (BSE) or element resolved (X-ray) imaging significantly, because – unlike the secondary electrons (SE), which are collected from the sample surface and used for normal imaging – BSE and X-rays are collected from the excitation volume. Due to the higher penetration depth of X-rays this is especially severe for elemental mapping by X-rays. Another problem imposed by the electrode porosity is the variation of the detection probability for the X-ray signal throughout the electrode. As the density of the material varies throughout the electrode, the excitation volume and therefore the amount of material contributing to the signal varies, too. Furthermore, the porosity induces a high surface roughness of the sample which modulates the X-ray signal. Therefore, the elemental information obtained by the X-ray signal cannot be quantified correctly and elemental maps obtained by this method may not correspond to the real elemental distribution in the sample. A limitation that does not only apply to SEM, but to all electron microscopy techniques and therefore also TEM, is the beam sensitivity of the commonly used PFSI polymer electrolyte [14–16]. But as the sensitivity of EDX for light elements such as fluorine, which is the predominant element in PFSI polymer electrolytes, is rather low, long recording times are necessary for mapping and hence beam damage of the sample becomes an important issue. These limitations restrict the characterization of the polymer electrolyte distribution to the micrometer range and care must be taken when interpreting the results. As the demand of industry for lower production costs has led to a significant decrease of the catalyst loading and therefore to a decrease in electrode thickness to the range of only a few microns [13], SEM on bulk cross-sections may only provide limited information for further optimization of the electrode structure.

Although TEM in principle suffers from the same beam damage problems as SEM, TEM has a number of advantages for the characterization of the polymer electrolyte distribution. TEM allows imaging of all parts of the electrode structure including the nanometer sized catalyst particles, which are in general not accessible by SEM. As samples need to be thinned to less than 100 nm to be transparent for the electron beam, pores between the catalyst agglomerates appear as voids in the catalyst structure and can therefore be imaged, too. Moreover, with energy filtered transmission electron microscopy (EF-TEM) another powerful technique is available for elemental mapping. In contrast to EDX, energy filtered transmission electron microscopy is more sensitive for light elements and allows acquisition of the whole image at the same time. This reduces the acquisition time from several hours to a few minutes and therefore minimizes beam damage of the sample.

However, sample preparation for TEM is a major obstacle, especially for highly porous systems such as PEMFC electrodes. Blom et al. proposed the adoption of a sample preparation technique which is generally used for biological samples [17]. To stabilize the structure of the electrode the membrane electrode assembly (MEA) is embedded in epoxy resin and then cut with an ultramicrotome using a diamond knife. As the epoxy resin infiltrates the pore space, the electrode structure is preserved during the sectioning process. Thus sections can be obtained, which are sufficiently thin (∼70–100 nm) for TEM analysis. The sectioning process furthermore yields sections of rather homogeneous thickness, which allows imaging of the whole cross-sectional area, including also the membrane.

Since the electrode structure is preserved by this preparation method and characterization of the membrane is possible, too, it is ideally suited for studying catalyst degradation processes during long-term operation [18–20]. All three articles report significant changes of the electrocatalyst and observed segregation of platinum particles in the membrane. The location of platinum particle segregation within the membrane seems to show a dependence on the operation potential. Akita et al. reported

segregation of Pt particles in the membrane close to the cathode side after aging at constant potential (1.0 V), while Xie et al. observed particle deposition in the membrane close to the anode during a life test of 1000 h at constant current (1.07 A cm^{-2}) and high humidity.

However, for the analysis of the polymer electrolyte distribution, infiltration with an epoxy resin has a significant drawback. Since the polymer electrolyte and the embedding resin have almost identical scattering contrast, the polymer electrolyte cannot be distinguished directly. As pores in the electrode structure may be filled by the polymer electrolyte or the embedding resin, it is also not possible to distinguish between open and closed pores (i.e. those filled by the polymer electrolyte). In this paper, we present different approaches to solve the contrast problem and suggest methods to characterize the polymer electrolyte distribution, which combine the advantages of the thin section technique with the possibility to image the polymer electrolyte distribution.

2. Experimental

MEAs used in this study were prepared by a hot spraying technique. The catalyst ink, consisting of the catalyst dispersed in a mixture of water, isopropanol and Nafion® solution (Aldrich), was sprayed on a heated (100 °C) Nafion® membrane, which has been boiled in 2% H_2O_2 and 2N H_2SO_4 for about 1 h, respectively.

Sample preparation for TEM followed the procedure described by Blom et al. [17]. A small piece was removed from the MEA and embedded in Araldite 502 resin (SPI Supplies Inc.). Subsequently, the resin was cured at 60 °C for at least 16 h. Sectioning of the embedded samples was carried out with a Reichert–Jung ultracut microtome at room temperature using a diamond knife. The sections were then transferred to copper grids and dried at room temperature for at least 48 h. Sections of 200–500 nm thickness and ultra-thin sections of 70–100 nm were prepared for SEM and TEM microscopy, respectively.

Thin sections were analyzed with a FEI Quanta 200 FEG environmental scanning electron microscope equipped with an energy dispersive X-ray detector for elemental analysis and mapping. To minimize interaction of the electron beam with the sample holder a specially designed holder was used, which supports the copper grids only on their outer rim (Fig. 1). Ultra-thin sections were examined with a Jeol JEM-3010 transmission electron microscope operating at 300 kV acceleration voltage with a LaB_6 cathode. The instrument is equipped with a gatan imaging filter (GIF) for energy filtered imaging and electron energy loss spectroscopy (EELS).

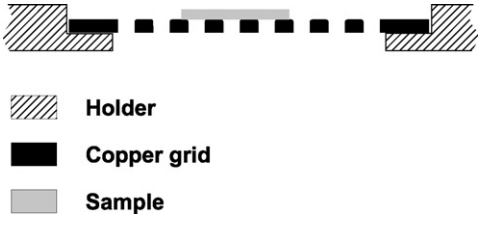

Fig. 1. Schematic representation (cross-section) of the sample holder for SEM analysis of thin sections.

3. Results and discussion

In the introduction it has been pointed out that infiltration of the electrode structure with epoxy resin has a significant drawback for imaging of the polymer electrolyte distribution. This is due to the very similar scattering contrast of the polymer electrolyte and the epoxy resin. There are basically two different approaches to solve this problem, which will be discussed in more detail in this section:

- Enhancement of the scattering contrast by selective insertion of heavy metal ions in either the polymer electrolyte or embedding resin (referred to as *staining techniques*).
- Elemental mapping of an element that is characteristic for either the polymer electrolyte or the embedding resin (referred to as *mapping techniques*).

3.1. Staining techniques

The polymer electrolyte in a fuel cell is exposed to rather harsh chemical and electrochemical conditions. Therefore, the polymer backbone of the polymer electrolyte must possess a high chemical stability, i.e. it must have a low reactivity. This property is highly unfavorable for the incorporation of staining agents into the polymer backbone itself. But staining can be realized via the ionic groups of the polymer electrolyte. The protonized form of the polymer electrolyte can be easily transferred to an ion exchanged form by exposing it to a solution containing a metal salt. It has been shown in literature that a wide variety of metal salts and even rather bulky organic cations like TBA^+ can be incorporated into PFSI polymer electrolytes [21,22], but other types of polymer electrolytes should behave similarly and therefore, this approach can be considered as a rather general approach, independent of the used polymer electrolyte.

To significantly increase the scattering contrast of the polymer electrolyte the staining agent should have a high electron density and a low charge to introduce as many additional scattering centers as possible. Therefore, cesium appears as an ideal staining agent and has also been used by Rieberer et al. to mark the sulfonic clusters of Nafion® membranes for examination with transmission electron microscopy [22]. Fig. 2 shows cross-sections of an unstained and Cs^+ stained MEA in comparison. In both images the interface between the membrane and the electrode appears sharp indicating that penetration of the membrane into the catalyst layer is low. A clear effect of the staining can be seen on the membrane of the cesium treated sample. The membrane of this sample appears to be speckled and stripes of more or less strongly contrasted regions can be found close to the electrode interface. Also the electrode of the stained sample appears to be darkened, when compared to that of the unstained sample. The staining in the electrode layer is most pronounced around the catalyst support particles indicating that the Nafion® ionomer is mainly covering the catalyst support particles but is not flooding large pores. This is in agreement with the results

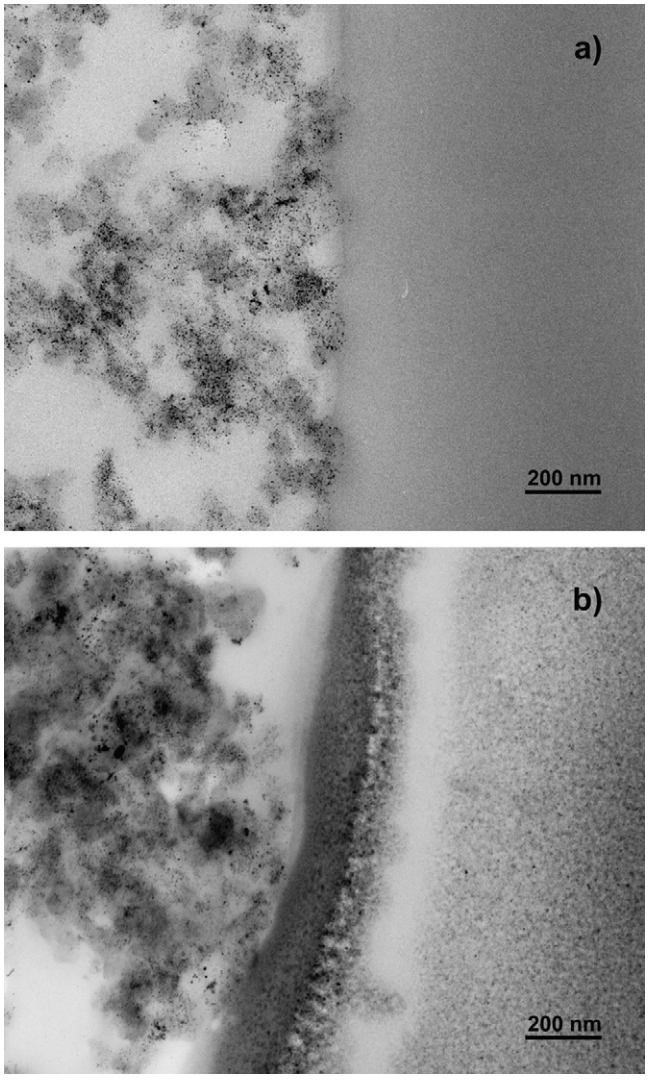

Fig. 2. TEM bright field images of an unstained (a) and Cs^+ stained (b) membrane electrode cross-section. Both images were taken at the membrane–electrode interface with the membrane shown on the right-hand side of the image.

of Gode et al. [5], supporting the assumption that the catalyst agglomerates are infiltrated by the polymer electrolyte in electrodes prepared from inks containing Nafion® in solution, as opposed to those containing colloidal Nafion® [11].

The different contrast regions in the membrane close to the membrane–electrode interface are most likely an artifact of the staining process and not a part of the inherent structure of the membrane. Immersion of the sample in the staining solution causes the membrane to swell. Since the membrane is constrained by the embedding media, it will distort to accommodate for its increased lateral dimensions. This distortion may then lead to contrast changes as observed in Fig. 2, by inhomogeneous drying and redistribution of the staining agent. However, it has also been reported that the membrane pretreatment process, which involves boiling of the membrane in H_2O_2 and H_2SO_4, causes an increase of the sulfonate group concentration at the membrane surface [15]. Therefore, the contrast changes observed at the interface may also be partly linked to changes in the sulfonate group concentration due to the membrane pretreatment process.

Staining artifacts could be mostly avoided if the ion exchange is carried out prior to the infiltration and sectioning process. However, cesium is washed out almost completely from pre-stained samples during the sectioning process. Therefore, cesium was replaced by barium, which is known to bond more strongly to sulfate or sulfonate groups. A sample that was pre-stained with barium is shown in Fig. 3. In contrast to samples pre-stained with Cs^+ a staining effect is clearly visible for the sample treated with Ba^{2+}. However, the staining effect is weaker than for cesium. This is mainly due to the higher charge of the barium ion (Ba^{2+}) compared to cesium (Cs^+), resulting in a lower amount of barium that can be incorporated into the polymer electrolyte. As expected the staining is more homogeneous when compared to cesium stained sample and no contrast variations were observed in the membrane, which indicates that staining artifacts were significantly reduced.

The speckling may be interpreted to arise from stained ionic clusters formed by segregation of the sulfonate groups containing side chains in the fluorocarbon matrix of the polymer backbone [22]. However, the high-resolution image shown in Fig. 4 reveals that the speckling arises from small nanocrystals in the membrane. Evaluation of the lattice fringes seen in Fig. 4 by Fourier transformation indicates that these nanocrystals are most probably barium fluoride. As both the sulfonic groups and the fluorinated polymer backbone are known to decompose under ionizing radiation [15], it is most likely that those crystals grow under the influence of the electron beam. Barium ions which are released from destroyed sulfonic groups may react with fluorine as the side chains and the polymer backbone degrade in the electron beam. Crystalline structures have also been observed in the

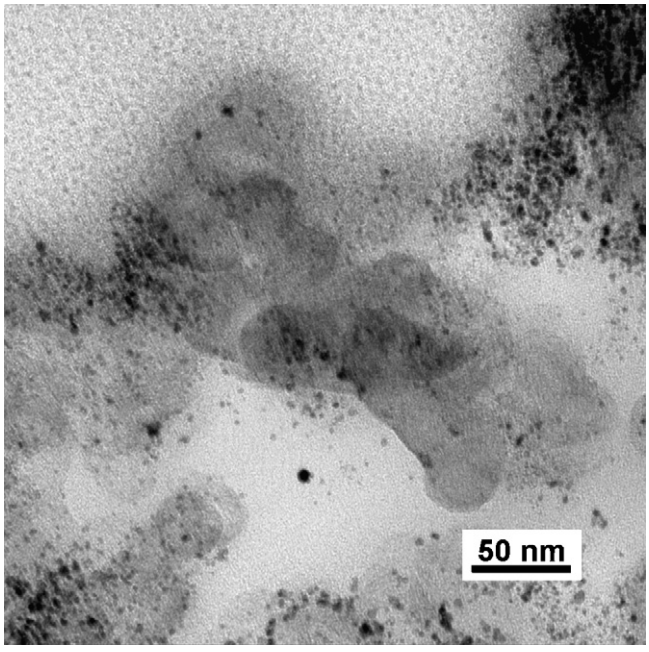

Fig. 3. TEM bright field images of an MEA exposed to $Ba(OH)_2$ solution before embedding in epoxy resin. The image shows the membrane–electrode interface with the membrane in its upper left corner.

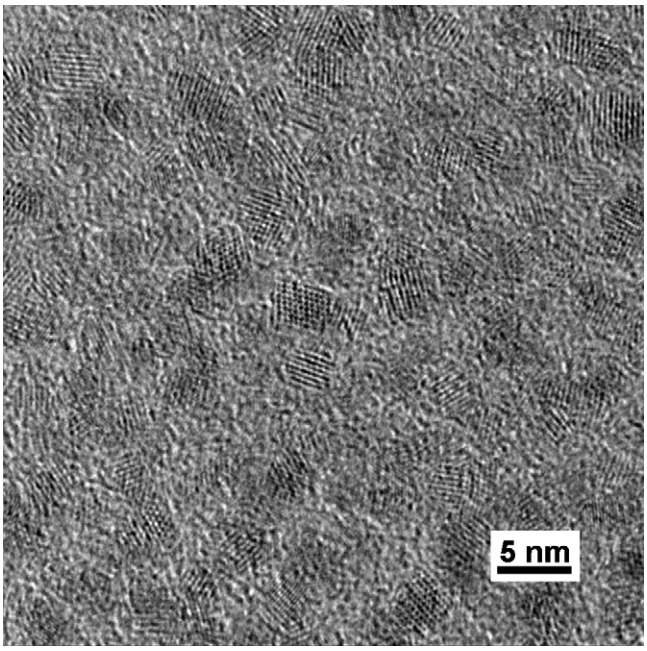

Fig. 4. High-resolution TEM bright field image of the Nafion® membrane doped with barium ions. Small crystalline regions can be found throughout the membrane whose lattice spacings fit well to BaF_2.

darkened regions of cesium stained samples, indicating that this phenomenon is not only limited to barium staining. It is therefore not possible to directly correlate the size of the "stained" regions to the size of the ionic clusters in PFSI membranes or recast films. However, the size of the barium fluoride clusters may be used to calculate the average number of sulfonate side chains contributing to their formation. The mean barium fluoride cluster size determined from Fig. 4 is about 2.9 nm. Assuming spherical symmetry for the barium fluoride clusters the average number of barium atoms in each cluster is 215. As each side chain in Nafion® contains only one sulfonate group and one barium ion bonds to two sulfonate groups for reasons of charge balance, the average number of side chains that contribute to the formation of the barium fluoride clusters is about 430. According to the results of Gierke et al., based on their cluster-network model of Nafion®, the number of sulfonate groups per ionic cluster is about 27 for a completely dried sample [24]. This means that on average at least 16 ionic clusters contribute to the formation of one barium fluoride cluster. This result is certainly a rough approximation, since it is based on several simplifications regarding the structure of Nafion® and the structure of the barium fluoride crystals. However, it demonstrates, that either significant structural rearrangement has to take place when the sample is exposed to the electron beam or percolation of ionic clusters does already exist in the non-humidified sample. Nevertheless, although significant structural rearrangement of the polymer electrolyte may occur in the TEM on an atomic and molecular level, microstructural changes of the electrode and membrane were not observed unless very high beam intensities were used. Furthermore, the staining experiment demonstrates that barium staining may be used to reduce fluorine loss from the electrode and membrane during electron microscopy analysis by binding fluorine into BaF_2 nanocrystals.

3.2. Elemental mapping

Elemental mapping techniques are an elegant alternative to staining experiments, as they do not require the insertion of a staining agent and are therefore less prone to artifacts. Instead, differences in the chemical composition can be used to distinguish the polymer electrolyte from the resin. For PFSI polymer electrolytes, which are most commonly used for PEMFCs and DMFCs, the fluorine signal can be used to visualize the electrolyte distribution. The sulfur signal, which arises from the sulfonate groups, is less suitable for elemental mapping as it overlaps with the platinum $M\alpha_1$ line [14] and sulfur impurities of the carbon support may be mapped as well. Therefore, in this study we have focused on the fluorine signal.

Electron microscopy allows the use of two different elemental mapping techniques, namely EDX and EFI. A major advantage of the EDX method is its wide distribution and its availability also for scanning electron microscopy. Both methods have advantages and limitations that are rather complementary to each other and therefore they are best used in combination to characterize the polymer electrolyte distribution. As already pointed out in the introduction, the resolution of the EDX method is rather limited due to the large excitation volume for X-ray generation, which can reach a few micrometers for materials of low density. Although the use of thin sections instead of bulk samples reduces the excitation volume and therefore improves the resolution, it is difficult to resolve fine details of the polymer distribution by EDX. As the sensitivity of EDX for light elements such as fluorine is rather low and the elemental information is recorded sequentially for each image point, recording times of several hours are necessary to obtain an elemental map, thereby introducing problems of sample drift and sample stability. This is partly compensated by the fact that EDX allows parallel recording of several elements, so that for instance elemental maps of platinum or ruthenium can be obtained at the same time. In contrast, recording times for energy filtered images are only in the order of a few minutes, but only one element can be mapped at a time. Furthermore, EF-TEM fails to record elemental maps of heavy elements such as platinum and can hence not be used for mapping of the catalyst. And while it offers a much higher resolution than EDX, it is difficult to obtain images at low magnification, since, except for the so-called omega filter; the energy filter introduces a rather large post magnification.

3.2.1. Fluorine mapping by EDX

Fig. 5 shows the SE and BSE image of a thin section of a fuel cell electrode as well as elemental maps for carbon (C), fluorine (F), platinum (Pt) and ruthenium (Ru). In the lower half of the image a part of the membrane is visible. Since the fluorine signal recorded for the membrane was much more intense than that of the electrode, a log-transform of the image intensity was necessary to visualize the fluorine content in the electrode. The fluorine map of the electrode shows a similar intensity distribution as the carbon map, indicating that the polymer electrolyte

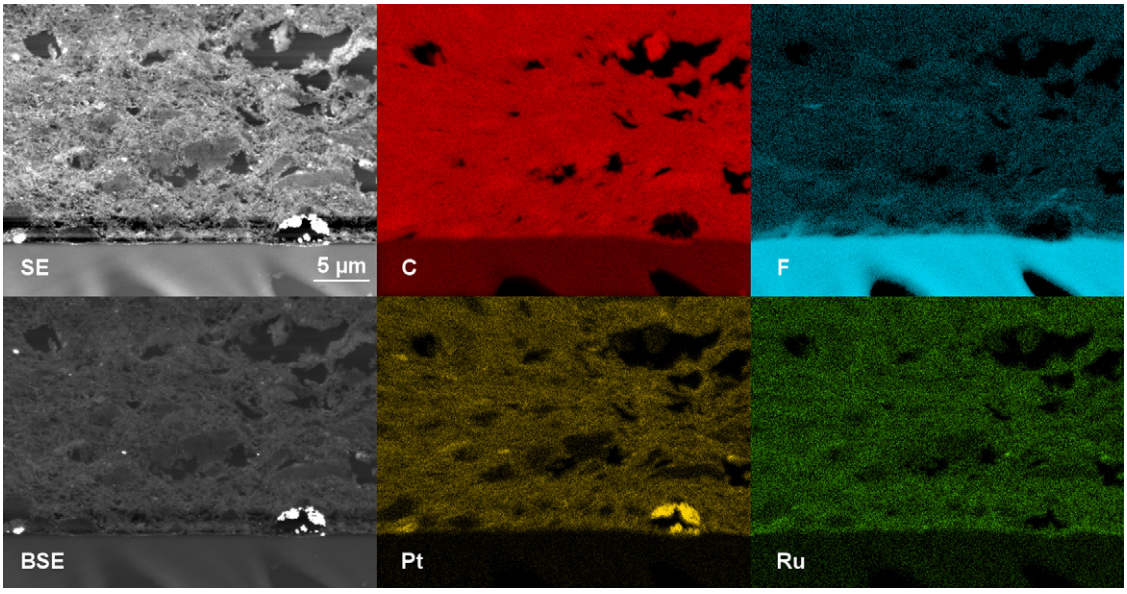

Fig. 5. SE and BSE micrographs of a DMFC anode catalyst layer and elemental maps for carbon (C), fluorine (F), platinum (Pt) and ruthenium (Ru) for the same region obtained by EDX mapping.

is homogeneously mixed with the catalyst. However, especially close to the interface with the membrane, a slightly higher fluorine concentration can be observed. It cannot be completely ruled out that this is caused to some degree by smearing of some polymer electrolyte of the membrane into the electrode during sectioning of the sample, therefore being an artifact of the sectioning process. However, it seems more likely that the higher fluorine signal is caused by segregation of the polymer electrolyte during the hot-spray preparation process. By this process the electrode layer is applied by spraying several layers of ink containing the catalyst and the polymer electrolyte onto a heated membrane. Capillary forces of the already sprayed layers may therefore tend to transport polymer electrolyte, which is still in the liquid phase of the ink, towards the membrane leading to a concentration gradient perpendicular to the electrode layer.

The platinum and ruthenium maps of the electrode, that have been acquired along with the fluorine map, reveal that the catalyst is not homogeneously distributed throughout the electrode layer. In particular, the platinum distribution shows agglomeration and some void regions, that do not correspond to holes in the electrode structure. Strong agglomeration of catalyst particles was also observed for other catalysts, including commercial ones. This is noteworthy, since no indication of such agglomeration was found by classical TEM analysis of dispersed powder samples of these catalysts. There are two reasons why TEM analysis of powder samples fails to detect large catalyst agglomerates. (i) TEM usually probes only a very small sample volume, (ii) particles of more than 100 nm in diameter can generally not be analyzed by TEM, as they are opaque to the electron beam. Therefore, it is not possible to differentiate between well dispersed catalyst particles on agglomerated catalyst support particles and large agglomerates of unsupported catalyst particles by TEM analysis of dispersed powder samples. As this method has become a standard characterization technique for dispersed catalyst samples, one should bare in mind, that dispersion information derived by this method may lead to inaccurate or erroneous results. BSE imaging and EDX mapping of catalyst thin-sections may provide additional information on the catalyst distribution and should become a recommended standard characterization procedure for dispersed catalyst samples.

3.2.2. *Energy filtered imaging (EFI)*

Elemental information can be obtained from energy filtered image data either by the three- or the two-window method [25]. For the three-window method, which was used in this work, three images are acquired. One at an energy corresponding to the characteristic loss feature of the element investigated (post-edge image) and two at energy losses slightly lower than the characteristic energy loss feature (pre-edge image). The latter images are used to construct a background image, which is subtracted from the post-edge image to obtain the elemental distribution.

EF-TEM uses only a relatively small fraction of the electrons illuminating the sample to form an energy filtered image. As a consequence, to keep recording times short, high electron doses are necessary during the exposure. Since high electron doses also accelerate the degradation of the polymer electrolyte, it is necessary to know at which rate this degradation takes place to make reliable interpretations of the obtained fluorine concentration maps. To determine the degradation rate, a sequence of electron energy loss spectra was acquired from the membrane at electron doses similar to that used for the acquisition of the energy filtered images. Fluorine losses of about 2.5% per minute were determined by integration of the intensity of the fluorine edge from the sequence of EEL-spectra. Since a typical acquisition of three energy filtered images – two pre-edge images for background correction and one post-edge image, that contains the elemental information – takes about 3 min (∼1 min for each image), the fluorine loss during acquisition is less than 10%. The effect of fluorine loss is further minimized, since the post-edge image is acquired first and the influence of the fluorine loss on

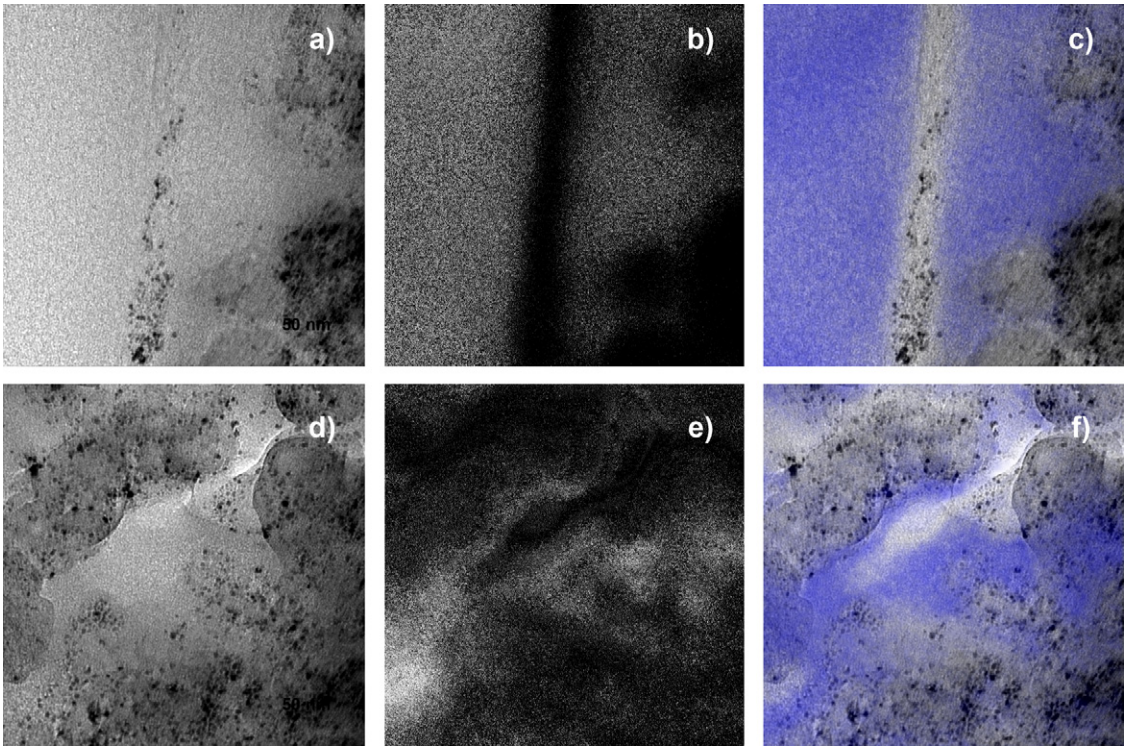

Fig. 6. Unfiltered transmission electron micrographs of the membrane electrode interface (a) and a part of the electrode layer (d). Images (b) and (e) show fluorine maps of these regions obtained by energy filtered transmission electron microscopy applying the three-window method. Bright parts in the image correspond to a high fluorine concentration. A superposition of the fluorine map with the unfiltered images is displayed in (c) and (f).

the pre-edge images should be negligible. This demonstrates that energy filtered imaging of the fluorine distribution in PEFCs is possible and that the results obtained are only slightly affected by fluorine losses during acquisition time.

Unfiltered transmission electron micrographs and the corresponding fluorine maps of a PEFC electrode at two different locations are shown in Fig. 6. The fluorine maps were obtained using the three-window method with pre-edge images at 643 and 670 eV and a post-edge image at 698 eV. All energy filtered images were recorded with a slit width of 25 eV and an exposure time of 30 s.

Images a–c were acquired directly at the membrane–electrode interface. A part of the membrane is visible in the left half of the images. The interface between the membrane and the electrode is clearly visible in the fluorine map (Fig. 6b) as a stripe of low fluorine concentration (dark color). On the right side of the interface some pore space is visible, that is completely filled by the polymer electrolyte, indicated by bright contrast or blue color in Fig. 6b and c. At image positions, where catalyst material is present, the signal of the fluorine concentration essentially drops to zero, because the volume of the cross-section at these sample positions is almost completely occupied by the catalyst and the support particles. However, in the lower right corner of the image a fluorine signal can also be detected in between two support particles, which lie in close proximity to each other, indicating that Nafion® can penetrate into the void space of the catalyst agglomerates.

Fig. 6d–f shows a part of the electrode structure further apart from the membrane–electrode interface. In contrast to the image taken at the membrane–electrode interface the pore space in the electrode layer is not completely filled by the polymer electrolyte. In some parts of the image the fluorine distribution can be seen to closely follow the contours of the catalyst support particles, indicating that the polymer electrolyte coats the catalyst and catalyst support particles. The catalyst agglomerates appear rather dense with no visible void space. Therefore, the void space inside the catalyst agglomerates must be significantly smaller than the thickness of the ultra-thin section (i.e. $\ll$100 nm). This is consistent with the agglomerate model described by Uchida et al. [11], who, based on mercury porosimetry data, assigned a pore range from 20 to 40 nm to pores inside the catalyst agglomerates. Due to the small volume of these pores, which might be occupied by the polymer electrolyte, the fluorine signal originating from parts inside the catalyst agglomerates is very low and cannot be clearly distinguished from experimental noise. Hence, so far it was not possible to clearly ascertain the extent to which the polymer electrolyte penetrates into the catalyst agglomerates. However, by optimization of the sample preparation and acquisition parameters the elemental sensitivity might be further improved, so that information of the fluorine distribution also from parts inside the catalyst agglomerates may be obtained.

4. Conclusion

It has been demonstrated that the combination of SEM and TEM imaging of thin and ultra-thin sections of membrane–electrode assemblies is a powerful tool to characterize the electrode structure of PEMFC.

Compared to bulk sections and bulk samples thin sections provide a much higher information level due to the preservation of the pore structure and smaller excitation volume in SEM. However, the detection of the polymer electrolyte is difficult because of its masking by the embedding resin and its instability in the electron beam.

Two approaches were proposed to distinguish the polymer electrolyte from the embedding media:

(1) Contrast enhancement by doping the polymer electrolyte with heavy metal ions.
(2) Mapping of the fluorine distribution by element sensitive imaging techniques (EDX mapping and EF-TEM).

Contrast enhancements by doping the polymer electrolyte with heavy metal ions revealed that the polymer electrolyte is mainly concentrated around the catalyst and catalyst support particles. However, contrast enhancements obtained by this method were too low to allow clear identification of the polymer electrolyte at higher magnification. Moreover, they are also likely to introduce artifacts, in particular inside the membrane due to swelling of the polymer electrolyte during the staining process.

EDX mapping and BSE imaging of MEA thin sections proved to be a suitable tool to study the catalyst dispersion also in the inside of large catalyst agglomerates, which is generally not accessible by classical TEM analysis of dispersed powder samples as particles exceeding about 100 nm in diameter cannot be transmitted by the electron beam. EDX fluorine maps of MEA thin sections could be obtained, too, but the count rate of the fluorine signal inside the electrode was low, providing not much detail of the polymer electrolyte distribution.

Further, it was demonstrated that EF-TEM can be successfully used to acquire element distribution maps of fluorine. With EF-TEM it was possible to resolve the fluorine distribution at resolutions where individual catalyst support particles can be distinguished. The polymer electrolyte was found to form a several nanometers thick coating on the catalyst and catalyst support particles inside the electrode layer, while close to the membrane–electrode interface complete blocking of pores was observed.

Acknowledgments

Financial support from the DFG and the Sino-German Center in Beijing in a joint project between the ZAE Bayern (Garching, Germany), the School of Chemistry (Tsinghua University, Beijing, China), and the Institute of Materials Science (Darmstadt University of Technology, Germany) are gratefully acknowledged.

References

[1] V. Gogel, T. Frey, Y.S. Zhu, K.A. Friedrich, L. Jorissen, J. Garche, J. Power Sources 127 (2004) 172.
[2] J. Nordlund, A. Roessler, G. Lindbergh, J. Appl. Electrochem. 32 (2002) 259.
[3] Z.B. Wei, S.L. Wang, B.L. Yi, J.G. Liu, L.K. Chen, W.J. Zhou, W.Z. Li, Q. Xin, J. Power Sources 106 (2002) 364.
[4] E. Antolini, L. Giorgi, A. Pozio, E. Passalacqua, J. Power Sources 77 (1999) 136.
[5] P. Gode, F. Jaouen, G. Lindbergh, A. Lundblad, G. Sundholm, Electrochim. Acta 48 (2003) 4175.
[6] E. Passalacqua, F. Lufrano, G. Squadrito, A. Patti, L. Giorgi, Electrochim. Acta 46 (2001) 799.
[7] M. Uchida, Y. Fukuoka, Y. Sugawara, N. Eda, A. Ohta, J. Electrochem. Soc. 143 (1996) 2245.
[8] G.C. Li, P.G. Pickup, J. Electrochem. Soc. 150 (2003) C745.
[9] J.H. Kim, H.Y. Ha, I.H. Oh, S.A. Hong, H.I. Lee, J. Power Sources 135 (2004) 29–35.
[10] S.J. Shin, J.K. Lee, H.Y. Ha, S.A. Hong, H.S. Chun, I.H. Oh, J. Power Sources 106 (2002) 146.
[11] M. Uchida, Y. Aoyama, N. Eda, A. Ohta, J. Electrochem. Soc. 142 (1995) 463.
[12] J. Xie, F. Garzon, T. Zawodzinski, W. Smith, J. Electrochem. Soc. 151 (2004) A1084.
[13] M.S. Wilson, S. Gottesfeld, J. Appl. Electrochem. 22 (1992) 1.
[14] M. Schulze, M. von Bradke, R. Reissner, M. Lorenz, E. Gulzow, J. Anal. Chem. 365 (1999) 123.
[15] M. Schulze, M. Lorenz, N. Wagner, E. Gulzow, Fresen. J. Anal. Chem. 365 (1999) 106.
[16] Z. Porat, J.R. Fryer, M. Huxham, I. Rubinstein, J. Phys. Chem. 99 (1995) 4667.
[17] D.A. Blom, J.R. Dunlap, T.A. Nolan, L.F. Allard, J. Electrochem. Soc. 150 (2003) A414.
[18] T. Akita, A. Taniguchi, J. Maekawa, Z. Sirorna, K. Tanaka, M. Kohyama, K. Yasuda, J. Power Sources 159 (2006) 461.
[19] E. Guilminot, A. Corcella, F. Charlot, F. Maillard, M. Chatenet, J. Electrochem. Soc. 154 (2007) B96.
[20] J. Xie, D.L. Wood, K.L. More, P. Atanassov, R.L. Borup, J. Electrochem. Soc. 152 (2005) A1011.
[21] S.T. Iyer, D. Nandan, B. Venkataramani, React. Funct. Polym. 29 (1996) 51.
[22] S. Rieberer, K.H. Norian, Ultramicroscopy 41 (1992) 225.
[24] T.D. Gierke, G.E. Munn, F.C. Wilson, J. Polym. Sci. Part B: Polym. Phys. 19 (1981) 1687.
[25] F. Hofer, W. Grogger, P. Warbichler, I. Papst, Mikrochim. Acta 132 (2000) 273.